JOURNAL OF MATERIALS SCIENCE **35** (2000) 1405–1412

Grain boundary strength in non-cubic ceramic polycrystals with misfitting intragranular inclusions (nanocomposites)

S. KOVALEV
Synergy Ceramics Laboratory, Fine Ceramics Research Association, Nagoya 462-8510, Japan
E-mail: skovalev@earthlink.net

T. OHJI, Y. YAMAUCHI
National Industrial Research Institute of Nagoya, Nagoya 462-8510, Japan

M. SAKAI
Department of Materials Science, Toyohashi University of Technology Tempaku-cho, Toyohashi 441-8580, Japan

The residual stress distribution in polycrystalline ceramics with thermal expansion anisotropy and misfitting intragranular dispersion is studied through micromechanical simulation. The effective grain boundary strength under remote tension is derived from the stability of a grain-boundary microcrack with thermal elastic residual stresses. This result is then applied to the strength and fracture properties of a two-phase nanocomposite (5 vol% SiC-Al_2O_3). The residual stresses from misfitting dispersion increase the effective grain boundary strength of the nanocomposite from 1.5 to 5 times more than that of the single-phase polycrystal, depending on the grain size of the matrix phase. The residual stresses reduce the instability range of microcrack precursors at grain junctions and increase the initial level of driving force for critical microcrack extension. Predicted strengthening of grain boundaries leads, in turn, to the superior inert strength of unnotched nanocomposite.

1. Introduction

Improvements in the mechanical properties of advanced ceramics achieved in the past decade have been properly analyzed and evaluated from the point of toughening. The experimental data for nanocomposites [1] have demonstrated, however, that the higher inert strength is attained by the rather modest toughness. Since the conventional fracture mechanics approach failed in providing an adequate explanation to this behavior, extensive research attention has been recently attracted to this issue [2–12].

The addition of a misfitting particulate phase is not a new concept for toughening. It operates through the crack-face bridging, crack deflection or bowing, along with the microcrack-related energy dissipation, etc. However, very high levels of strengthening have never been reported for brittle particulate composites by this approach. The conventional microstructural design for toughening two-phase composites has mainly been made through increasing the volume fraction and size of reinforcement [13], clearly contradicting the concept of nanocomposite, where the dispersion is fine and its volume fraction is low [5]. Several mechanisms have been proposed for the enhanced inert strength and the creep resistance of nanocomposites; these include thermal residual stresses, change in grain boundary morphology, dislocation activity, enhanced interfacial fracture energy, etc. (see review paper [14]). The present study addresses the analysis of the most evident but still not fully understood mechanism of strengthening, namely, the thermal residual stresses in a SiC-Al_2O_3 nanocomposite.

Thermal residual stresses in two-phase nanocomposites have been examined by model calculations and experimental measurements [3, 4, 6, 9–11]. The analytical estimates are based, as a rule, on the concept of a mean residual stress field in matrix, as proposed by Mori and Tanaka [15]. This analysis smears local stress variations over a representative volume. In consequence, the mean stress is tensile in matrix for inflated dispersion and compressive for deflated one. The residual stresses observed in nanocomposites have also been limited to the averaged ones [3, 9, 10]. The experimental techniques available are accurate enough for discerning the uniform stress state inside the particulate phase, but obviously insufficient for resolving local stress concentrations, the most important factor for controlling the microfracture.

The influence of residual stresses on fracture toughness of two-phase composite was estimated by Cutler

and Virkar [16] for WC-Co alloys. Similar approach was made by Taya *et al.* [17] for TiB_2-SiC composite and by Levin *et al.* [4] for SiC-Al_2O_3 nanocomposite. The local stress distribution was neglected in these models, and the macroscopic toughness increment in a periodic residual stress field was calculated in the one-dimensional stress intensity formula for uniformly distributed tractions applied to the crack faces.

It is clear that the residual stress simulations and its measurements have been exclusively aimed at the influence of mean microstress on macro-toughness, while the micromechanical details have been unexplored. Levin *et al.* [4] pointed out a possible interaction of thermoelastic microstresses of a parent polycrystal (matrix) with the misfitting stresses of dispersion. Pezzotti *et al.* [9] addressed a possible hindering of grain boundary microcracks by localized stresses. Hoffman and Rödel [10] compared different experimental observations and concluded the local residual stresses to be responsible for the strengthening of nanocomposites. Chimani *et al.* [18] reported a method for reducing residual stress singularities at structural bimaterial junctions by introducing a misfitting reinforcement with a characteristic diameter close to that of the influencing region of the singular stress. This result suggests what happen on the microstructural level inside the matrix grain "reinforced" by misfitting nanodispersion.

The present study is directed to a micromechanical simulation for a model nanocomposite, a brittle non-cubic polycrystal reinforced by misfitting intragranular dispersion. The grain boundary is supposed to be the weakest link in the parent single-phase non-cubic polycrystal. The influence of misfitting intragranular dispersion on the extension of a grain boundary microcrack will be examined to understand the unnotch strength of the model nanocomposite*.

2. Fracture mechanics modeling

A micromechanical simulation is performed through finite element analysis for a model particulate nanocomposite. This allows taking into account both the inclusion-matrix thermal expansion misfit and the thermal expansion anisotropy (TEA) of matrix grains. The extension stability of a grain-boundary microcrack under applied and residual stresses is determined from an energy criterion for microcrack extension. A general criterion for crack extension stability under combined remote and residual stresses is considered, and then the strengthening of model nanocomposites is discussed.

2.1. Coupled effect of residual thermal stresses and applied remote load on crack extension stability

The combined action of residual stress and the applied load on crack propagation has been commonly characterized by adding their stress intensity factors [19]. However, this approach fails whenever the crack faces keep contact, where the stress intensity becomes negative. This difficulty may be overcome by utilizing an alternative approach; the general energy approach by Eshelby [20].

When an elastic body containing a crack is under the action of residual thermal stresses and an applied remote displacement, the total energy is written by

$$U_{\text{tot}} = U_{\text{tot}}^{(1)} + U_{\text{tot}}^{(2)} + U_{\text{int}} \tag{1}$$

where U_{r} is the residual strain energy resulting from the thermal distortion in the absence of external loading, U_{a} the strain energy for applied loading in the absence of residual distortions, and U_{i} the interaction energy [20]. Suppose s_{ij} and t_{ij} are the elastic strain and stress tensors for the residual field, and ε_{ij}, σ_{ij} are the elastic strain and stress tensors for the applied load, respectively. The elastic strain energies of (1) are, then, expressed by

$$U_{\text{tot}}^{\text{el}} = \frac{1}{2}\int_V t_{ij}s_{ij}\mathrm{d}V - \int_S p_i u_i \mathrm{d}S = -\frac{1}{2}\int_V t_{ij}s_{ij}\mathrm{d}V \tag{2a}$$

$$U_{\text{a}} = \frac{1}{2}\int_V \sigma_{ij}\varepsilon_{ij}\mathrm{d}V, \tag{2b}$$

while the interaction energy is defined by

$$U_{\text{i}} = \int_V t_{ij}\varepsilon_{ij}\mathrm{d}V \left(\equiv \int_V \sigma_{ij}s_{ij}\mathrm{d}V \right) \tag{3}$$

The strain energy release rate during crack extension is defined by

$$F_{\text{I}}^{\text{el}}(s) = -\frac{\partial U_{\text{tot}}^{\text{el}}}{\partial s}; \tag{4}$$

where ξ is the dimensionless crack length. The general condition for equilibrium cracking is given by

$$G(\xi) \equiv G_{\text{r}}(\xi) + G_{\text{a}}(\xi) + G_{\text{i}}(\xi) = 2\Gamma \tag{5}$$

in terms of the fracture energy Γ. In (5), G_{r}, G_{a}, and G_{i} are the respective components of residual, applied and interaction strain energy release rates calculated by (1) and (4). Γ is assumed to be constant for elastic brittle materials. From the energy conservation law in the equilibrium condition, the strain energy release rates G_{r} and G_{a}, are confirmed to be always non-negative, while G_{i} is either positive or negative. Rewriting (5)

* The scope of the present model is limited to the nanocomposites containing mainly intragranular inclusions. The results of simulation, thus, may not be applicable to the cases where inclusions are occluded on the grain boundaries, where, obviously, other strengthening mechanisms are in effect.

defines the critical driving force, $R(\xi)$, for the crack of length ξ in equilibrium;

$$R(\xi) \equiv G_a(\xi) = 2\Gamma - G_i(\xi) - G_r(\xi) \qquad (6)$$

The critical driving force $R(\xi)$ is often referred to as the R-curve. If a residual distortion is absent or has been relieved, G_a is equal to 2Γ, and (6) reduces to the criterion for brittle fracture. It is worthy of note in (6) with a negative interaction energy G_i that the presence of residual stresses can increase the driving force $R(\xi)$ relative to the fracture energy 2Γ, leading to toughening the material.

2.2. Model for grain-boundary microcracking in nanocomposite

The problem of microcracking in brittle materials has been extensively studied by the use of micromechanical fracture models [21–29]. Past applications mostly have been linked to the theoretical prediction of spontaneous microcracking in non-cubic polycrystals and particulate composites.

A modified model, originally proposed by Clarke [23], is employed in the present calculations. This model consists of a symmetric array of foursquare grains with anisotropic thermal expansion. They are embedded in an isotropic matrix with averaged thermal expansion (Fig. 1). The arrows in Fig. 1 indicate the directions of principal thermal deformations during cooling down the model array. This orientation of grains, representing the case of symmetric tilt boundaries, enforces the microcrack initiation at the four-grain junction. The isotropic polycrystalline matrix, the dimensions of the outer boundaries being supposed infinite, constrains the grain ensemble. Only 1/4 of the model was numerically analyzed due to the symmetry. The dimensions of the numerical model are shown in Fig. 2. Since the most residual strain energy is concentrated in the close vicinity of the grains, the isotropic matrix was terminated in its dimension at $x = 5D$ in the present numerical model. In subsequent simulations, this model (Fig. 2A) represents a single-phase polycrystal, being referred to as M0.

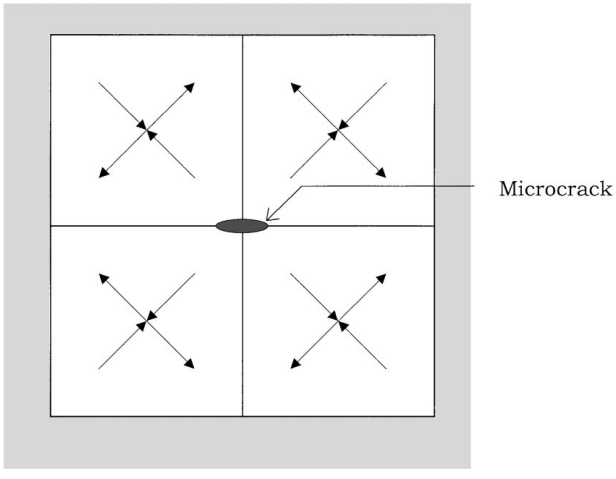

Figure 1 A model of grain-boundary microcracking due to thermal expansion anisotropy (Clarke, 1980). The arrows indicate the principal thermal deformations of grains, the grayed area represents an isotropically smeared polycrystal.

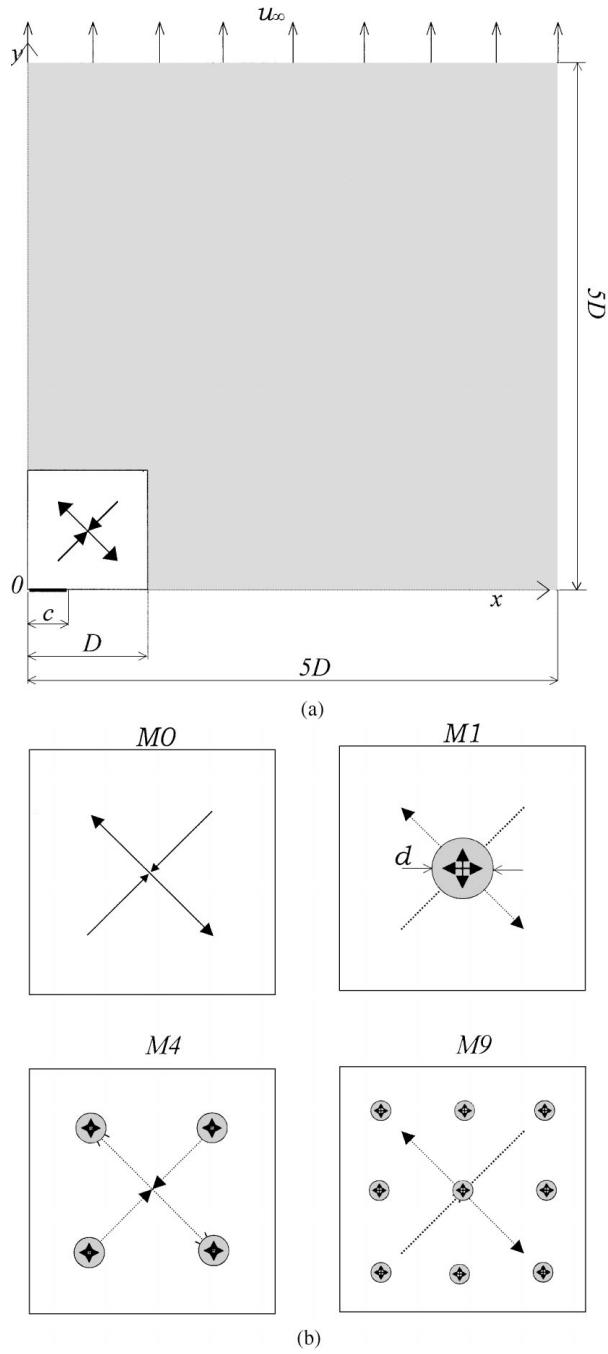

Figure 2 (A) One-quarter solid model used in the numerical simulations of a grain-boundary microcrack, the half-length of which is denoted by c (the grain model M0 is shown). The boundary conditions of symmetry are imposed on the sides $x = 0$ and $y = 0$. The side $x = 5D$ is free and a uniform tension u_∞ is applied on the side at $y = 5D$. (B) The model M0, and the models M1, M4 and M9 with $f_0 = 0.05$.

For two-phase composites with misfitting intragranular inclusions, the model M0 is modified by adding a regular array of circular inclusions. The model composites with various sizes of inclusion were investigated by keeping the volume fraction f_0 of the dispersion constant. This volume fraction in two-dimensional composite models is defined as the ratio of the total area of inclusions and that of grains. Accordingly, the diameter, d, of the inclusion, as shown in Fig. 2B, obviously depends on the number of inclusions per grain in the following manner;

$$d = \frac{D}{n}\frac{2}{\sqrt{\pi}}\sqrt{f_0} \qquad (7)$$

TABLE I Thermoelastic properties of the model composite

Phase	Elstic modulus, GPa	Poisson's ratio	Maximum thermal expansion coefficient, $\times 10^{-6}/^{\circ}$C	Minimum thermal expansion coefficient, $\times 10^{-6}/^{\circ}$C
Dispersion (SiC)	400	0.24	4.45	4.45
Matrix grain (Al_2O_3)	350	0.23	9.5	8.6
Matrix average (Al_2O_3)	350	0.23	9.05	9.05

where D is the grain size and n is the number of inclusions along the axis x (or y) in the array to make the total number of inclusions per grain of n^2. The composite models with $n = 1$, 2, and 3 referred to as Mn^2, that is, M1, M4, M9, are shown in Fig. 2B. Thus, the focus is on the influence of average size of the dispersion of constant volume fraction, while possible scatter in size of individual inclusions is neglected. Some material properties used for the present thermoelastic analyses are listed in Table I.

The strain energy release rates of (5) are rewritten as follows for the model shown in Fig. 2:

$$G_{\mathrm{r}}(\xi) = Dg_{\mathrm{r}}(\xi) \tag{8}$$

$$G_{\mathrm{a}}(\xi) = D\sigma_{\mathrm{a}}^2 g_{\mathrm{a}}(\xi) \tag{9}$$

$$G_{\mathrm{i}}(\xi) = D\sigma_{\mathrm{a}} g_{\mathrm{i}}(\xi) \tag{10}$$

where $\xi = c/D$ is the relative grain-boundary microcrack length, σ_{a} is the critical nominal stress induced by the critical applied remote displacement, u_∞, (see Fig. 2A) and approximated to be

$$\sigma_{\mathrm{a}} \approx \frac{\hat{E}u_\infty}{5D} \tag{11}$$

where $\hat{E}$ is the mean Young's modulus of the composite. The dependencies of G_{a} on $(\sigma_{\mathrm{a}})^2$ and of G_{i} on σ_{a} directly follow from (2b) and (3), respectively. In (8)–(10), g_{r}, g_{a} and g_{i} are the respective strain energy release rates normalized by D and σ_{a}. These functions, which depend on the geometry of the model, are calculated numerically. The substitution of (8)–(10) into (5) gives the following equation for the grain-boundary microcrack in a critical state;

$$g_{\mathrm{a}}(\xi)\sigma_{\mathrm{a}}^2 + g_{\mathrm{i}}(\xi)\sigma_{\mathrm{a}} + g_{\mathrm{r}}(\xi) = \frac{\Gamma_{\mathrm{gb}}}{D} \tag{12}$$

where Γ_{gb} is now the grain-boundary fracture energy. Solving (12) with respect to σ_{a} gives the critical nominal stress (the grain boundary strength) for the grain ensemble. The details of numerical analysis are outlined in Appendix.

3. Results and discussion

3.1. Residual stress distribution

The thermal residual stress distributions along the grain boundary of the single-phase and composite models are compared in Fig. 3 by normalizing the residual stresses with the nominal polycrystalline TEA stress, s_0;

$$s_0 = E(1+\nu)\Delta\alpha\Delta T \tag{13}$$

where E is the Young's modulus and ν the Poisson's ratio of the matrix, ΔT the cool-down interval of thermal stress build-up, and $\Delta\alpha$ is the difference between the maximum and the minimum thermal expansion coefficients of the anisotropic matrix grain (see Table I).

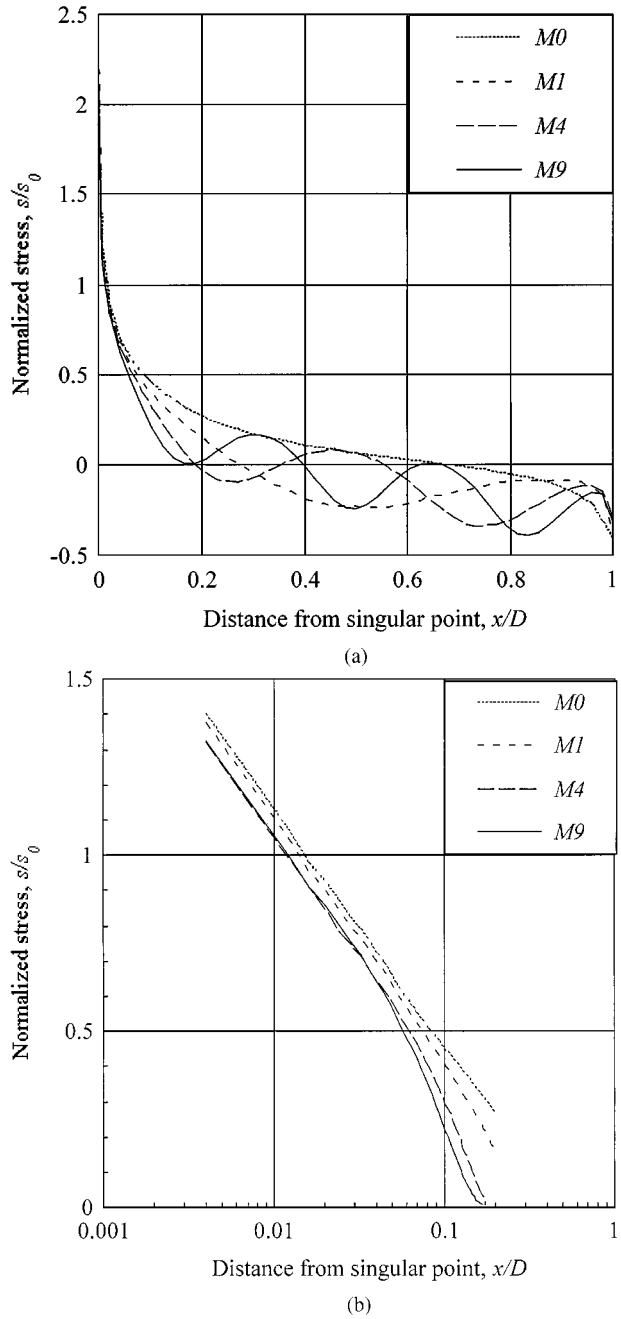

Figure 3 (A) The normalized thermal residual stress along the grain boundary, and (B) its semi-logarithmic plot in the vicinity of grain junction. The parameters for logarithmic best fit in $-2.5 < \log x/D < -1.5$ are listed in Table II. The nominal thermal stress $s_0 = 378$ MPa of Al_2O_3 was used.

The cool-down interval ΔT was simply taken to be 1000°C. The normal stress distribution for the model M0 is similar to that previously published [23, 26, 27]. The symmetric tilt boundary in the polycrystal is under tension near the four-grain junction, where the stresses are singular, while it is under compression in the region of about $x > 0.7D$. The addition of 5 vol% (equivalent to $f_0 = 0.05$ in (7)) of the second phase dispersion with lower thermal expansion (SiC) obviously reduces the spatial extent of the tensile region near the singular point (models M1, M4, or M9). The rest of grain boundary is under mixed tension-compression, depending on the number of misfitting inclusions. A semi-logarithmic plot of stresses in the near-singular region confirms a logarithmic singularity (Fig. 3B), established previously in similar problems (e.g., [22, 23, 27]). The present simulation, naturally, concluded none of reduction in the singularity via misfitting dispersions as seen in Fig. 3 and Table II.

The residual strain energy release rate curves, $G\mathrm{r}(\xi)$, are shown in Fig. 4 for different models with $D = 10\ \mu$m. The curve for the single-phase model M0 has a rising ($\mathrm{d}G_\mathrm{r}/\mathrm{d}\xi > 0$) and a falling ($\mathrm{d}G_\mathrm{r}/\mathrm{d}\xi < 0$) regions which prescribe unstable and stable microcrack extensions, respectively. The microcrack length, ξ_m, that yields the maximum G_r-value, separates the unstable ($0 < c/D < \xi_\mathrm{m}$) and stable ($\xi_\mathrm{m} < c/D < 1$) microcrack precursors in the cooled-down material. This curve is similar to the Lange's [21] generalized strain

TABLE II Parameters of logarithmic best fit, $s/s_0 = A + B\lg(x/D)$, for different models (Fig. 5B)

Model	A	B
M0	−0.517	−0.282
M1	−0.592	−0.304
M4	−0.542	−0.289
M9	−0.598	−0.306

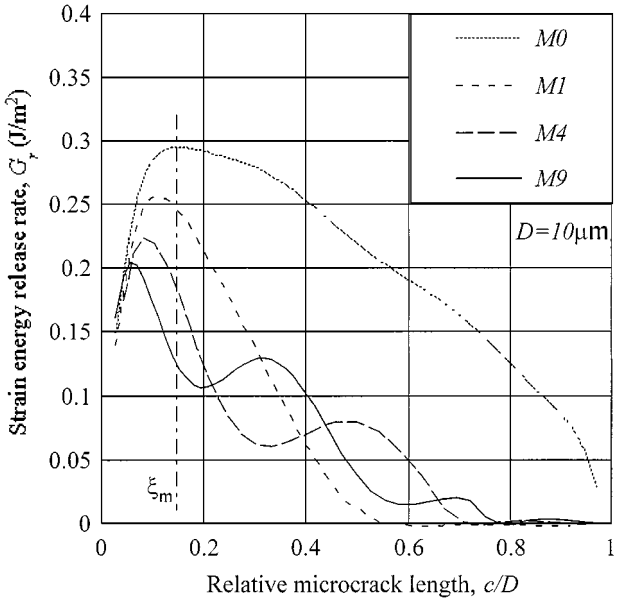

Figure 4 The thermal strain energy release rate of a grain-boundary microcrack for the model of single-phase polycrystal (M0) and two-phase composites with intragranular inclusions (M1, M4, and M9).

TABLE III Characteristic parameters for thermally induced microcracking

Model	ξ_m (see Fig. 4)	D_safe (μm)
M0	0.169	102
M1	0.110	117
M4	0.087	134
M9	0.060	146

energy release rate curve for a microcrack in a localized residual stress field. In the absence of applied displacement u_∞, and hence $\sigma_\mathrm{a} = 0$, (12) can be written by

$$g_\mathrm{r}(\xi) = \frac{\Gamma_\mathrm{gb}}{D} \tag{14}$$

and then,

$$D_\mathrm{safe} = \frac{\Gamma_\mathrm{gb}}{g_\mathrm{r}(\xi_\mathrm{m})} \tag{15}$$

where D_safe is the so-called microcrack-safe grain size [21]. It indicates the upper limit of grain size below which no spontaneous microcrack extension is possible during cooling down irrespective of the precursor length in non-cubic polycrystal. The model M0 for alumina with $\Gamma_\mathrm{gb} = 3$ J/m^2 gives $D_\mathrm{safe} = 102\ \mu$m[†].

The addition of misfitting dispersion of 5 vol% markedly changes the shape of residual strain energy release rate curve (see the curves M1, M4, and M9 in Fig. 4). Both the range of extension instability, $0 < c/D < \xi_\mathrm{m}$, and the peak value $G_\mathrm{r}(\xi_\mathrm{m})$ are reduced while the respective microcrack-safe grain sizes increase (see Table III). The misfitting dispersion, thus, reduces the population of potentially strength-controlling defects in the composite relative to the single-phase polycrystal. For rather large size microcracks, $c/D > 0.5$, the residual strain energy release rate progressively vanishes, as seen in Fig. 4, since the misfitting dispersion causes a microcrack closure which never occurs in the single-phase model.

3.2. The extension stability of a microcrack under uniaxial tension

The equilibrium microcrack in a residually stressed material under a remote uniaxial tension, as shown in Fig. 2, is defined by (12). If a preexisting defect of size ξ_0 falls in the range of $0 < \xi_0 \leq \xi_\mathrm{m}$, the solution of (12) at $\xi = \xi_\mathrm{m}$, where ξ_m is the crack length yielding the first maximum on the $g_\mathrm{r}(\xi)$ curve, gives a conservative estimate for grain-boundary strength $\sigma_\mathrm{gb}(\equiv \sigma_\mathrm{a})$:

$$\sigma_\mathrm{gb} = \frac{\sqrt{g_\mathrm{i}^2(\xi_\mathrm{m}) - 4g_\mathrm{a}(\xi_\mathrm{m})(g_\mathrm{r}(\xi_\mathrm{m}) - \Gamma_\mathrm{gb}/D)} - g_\mathrm{i}(\xi_\mathrm{m})}{2g_\mathrm{a}(\xi_\mathrm{m})} \tag{16}$$

The calculated results for the models with four different grain sizes are shown in Table IV. The grain-boundary

[†] Grain-boundary fracture energy is estimated as a half of the fracture energy of a single crystal [30]

TABLE IV Grain boundary strength of non-cubic polycrystalline nanocomposites

Model	Grain-boundary strength (MPa)			
M0	37.5	223	649	2130
M1	112	297	823	2690
M4	158	342	916	2980
M9	213	424	1110	3610
Grain size, D (μm)	100	50	10	1

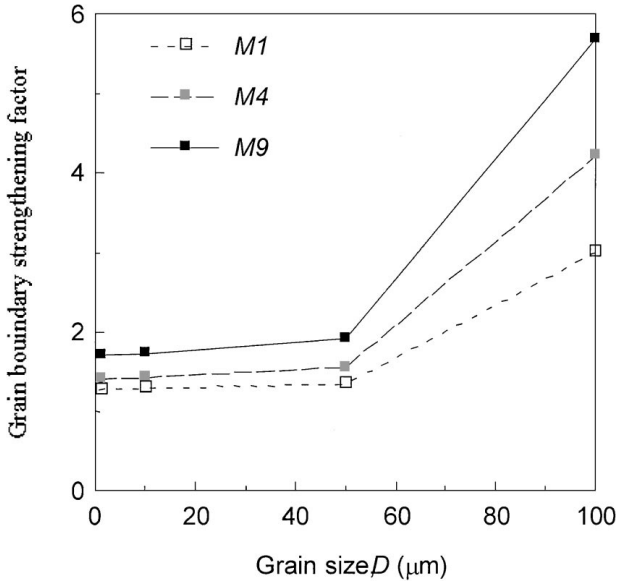

Figure 5 The grain-boundary strengthening factor (the ratio of grain boundary strengths of the composite and the single-phase polycrystal).

strength of all the model polycrystals naturally decreases with increasing the grain size. However, the ratio of strengths of composite and single-phase polycrystal is larger for the coarse-grained material than for the fine-grained one, as shown in Fig. 5. The grain-boundary is strengthened about 1.5 times in average in the range from 1 μm to 50 μm of grain size and about 5 times for grains close to 100 μm in diameter. This grain-size effect implies that the strengthening via intragranular dispersion is highly enhanced as the grain-size progressively increases and reaches the microcrack-safe limit of D_{safe} (= 102 μm for alumina matrix).

The grain-boundary strength of the model composites is examined furthermore in terms of the extension stability. Fig. 6 demonstrates the micro R-curve behaviors (6) of the grain-boundary microcrack for the model materials with two different grain sizes, D, of 10 μm (Fig. 6A) and 100 μm (Fig. 6B). The initial crack length ξ_0 for each curve is assumed to equal the value of ξ_{m} of the respective models. Note that the R-curve for the single-phase model (M0), being always less than 1.0, i.e., $G_{\text{a}}(\xi) < \Gamma_{\text{gb}}$, indicates embrittling the polycrystal by TEA residual stresses. Misfitting dispersion suppresses in part the TEA stresses, which is reflected by the rising R-curves for all the model composites. The grain-boundary strengthening is attained by the increment of the critical microcrack driving force and the decrement of the initial microcrack size, ξ_0. The

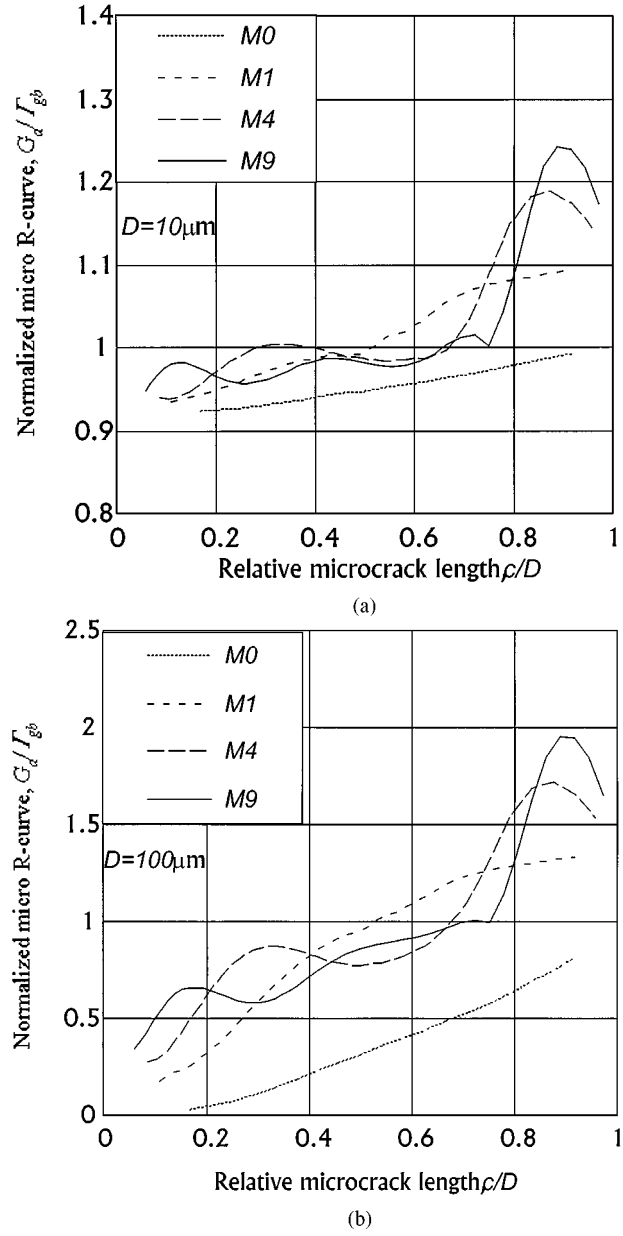

Figure 6 The normalized micro R-curves for the grain size of (A) 10 μm, and, (B) 100 μm. The respective R-curves initiate at ξ_{m}, shown in Table III. Note the difference in the scale of vertical axes of (A) and (B).

nanodispersion strengthening rises with grain size, as seen in Fig. 6, through the compensating contribution of misfitting dispersion against the TEA stress. Obviously, this strengthening effect of misfitting dispersion will be enhanced when the TEA stresses are relief via annealing of nanocomposites.

The positive R-curve effect, i.e. $G_{\text{a}}(\xi) > \Gamma_{\text{gb}}$, for a grain-boundary microcrack in nanocomposite appears only after a certain microcrack extension to about a half of the grain facet, D/2, as seen in Fig. 6. In addition to this characteristic of importance, the rising R-curves meander with crack extension, implying, a rather complicated stable/unstable crack extension. This extension behavior is seen for all the model composites except the M1 whith the largest grain size of 100 μm (Fig. 6B). The normalized R-curve ($G_{\text{a}}/\Gamma_{\text{gb}}$) of M1 exceeds 1.0 at the microcrack length which completely relieves the residual strain energy (see Fig. 4) associated

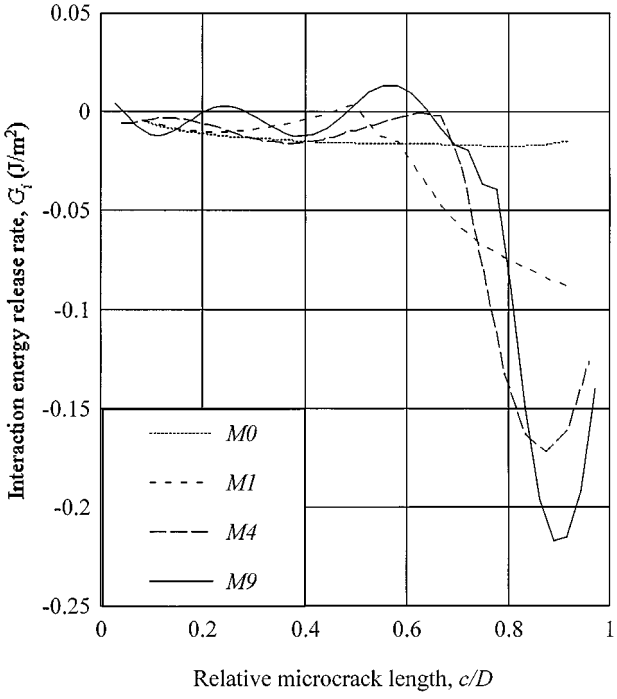

Figure 7 Interaction energy release rate curves G_i for a remote uniform tension ($u_\infty = 0.0143$ μm) applied on the model composites with the grain size of $D = 10$ μm.

with the microcrack closure via misfitting dispersion. As suggested in (12), the toughening is always attributed to the negative interaction strain energy release rate. In order to demonstrate this point, the interaction strain energy release rates, $G_i(\xi)$, are compared in Fig. 7. As a matter of fact, the negative interaction energy (or toughening) becomes significant after the microcrack leaves most of misfitting inclusions "in the wake", which is similar to the mechanics of transformation toughening [31]. It should be noted, however, that in real nanocomposites the fracture process, in view of enhanced stability of the grain-boundary microcracks, in most cases would rather switch to transgranular mode.

4. Conclusions

The modification of residual microstresses by the addition of misfitting dispersion of intragranular size to a non-cubic polycrystal has been examined as a candidate for possible strengthening mechanism of nanocomposites. The "toughening" through residual distortion has been properly analyzed via the interaction energy. The following conclusions are drawn from the model composites with misfitting (inflated) intragranular inclusions in a non-cubic polycrystal simulating a prototype material of 5 vol% SiC-alumina nanocomposite:

1. Second-phase misfitting intragranular dispersion increases the resistance to microcracking in non-cubic polycrystals with thermal expansion anisotropy via the reduction of both the spatial extent of microcrack instability at grain junction and the maximum residual strain energy release rate. This in turn limits the population of microcrack precursors and increases the microcrack-safe grain size.

2. The change in the extension stability of microcrack in the residual stress field improves grain boundary strength. The grain-boundary strengthening by misfitting dispersion is achieved to 1.5 times over the monolithic material for fine-grained and to about five times for coarse-grained polycrystals. The increase in grain boundary strength leads, in turn, to the inert strength enhancement observed for unnotched nanocomposite specimens and explains the transgranular appearance of the fracture surface.

3. The favorable influence of nanodispersion on the grain-boundary strength will be better realized by weaker anisotropy in the thermal expansion of matrix polycrystal. The experimentally observed increase in the inert strength of nanocomposite after annealing may be resulted from the relief of a part of total thermal residual stresses, which is attributed to thermal expansion anisotropy.

4. The rising R-curve behavior of grain-boundary microcrack in the model composites is more pronounced for a deeper microcrack. This resistance curve leads to toughening the nanocomposite only with coarse-grained polycrystals. For fine grain sizes, the nanocomposite, despite the notable increase in the grain-boundary strength, remains brittle, or even becomes more brittle than the parent single-phase polycrystal.

Appendix: Details of finite element calculations

ANSYS‡ Revision 5.2/5.3 finite element software was used in the calculation. PLANE42 element with plane strain option has been used in the model. All the boundaries between different materials (inclusion-grain and grain-matrix) were modeled as a double-noded coupled interfaces to prevent averaging of stress and strain across the boundary. The conditions of general contact have been introduced along the microcrack faces by the use of CONTAC48 element. The degree of mesh refinement utilized near the singular points of the grain junction and near the microcrack tip was selected in the range from 1/1440 to 1/2160 of the matrix grain size D for different models (M0–M9).

The elastic strain energies for the residual field and for the applied loading together with the respective interaction energy were calculated by the numerical integration of finite element results for elastic stresses and strains, (2) and (3). The energy release rate has been determined similarly to the virtual crack extension method of Parks [32]: a core of the finite elements within a fixed radius around the microcrack tip was shifted to a new position along the prospective microcrack path and the strain energy release rate was calculated simply by the finite differences. The core size of about $D/50$ and the crack tip shift of $D/1500$ were chosen after a careful investigation of the convergence to ensure the accuracy of 1% in the strain energy release rate calculations.

Acknowledgement

This work has been carried out as a part of the Synergy Ceramics Project under the Industrial Science

‡ Copyright by SAS IP as an unpublished work.

and Technology Frontier (ISTF) Program promoted by AIST, MITI, Japan. Under this program, part of the work has been funded through NEDO. S. Kovalev, T. Ohji, and Y. Yamauchi are members of the Joint Research Consortium of Synergy Ceramics.

References

1. K. NIIHARA, *J. Cer. Soc. Jap.* **99** (1991) 974.
2. J. ZHAO, L. C. STEARNS, M. P. HARMER, H. M. CHAN and G. A. MILLER, *J. Am. Cer. Soc.* **76** (1993) 503.
3. I. LEVIN, W. D. KAPLAN, D. G. BRANDON and T. WIEDER, *Acta Metall. Mater.* **42** (1994) 1147–1154.
4. I. LEVIN, W. KAPLAN, D. BRANDON and A. A. LAYYOUS, *J. Am. Cer. Soc.* **78** (1995) 254–256.
5. G. PEZZOTTI, T. NISHIDA and M. SAKAI, *J. Cer. Soc. Jap.* **103** (1995) 901–909.
6. M. J. HOFFMAN, M. STERNITZKE, J. RÖDEL and R. J. BROOK, in "Fracture Mechanics of Ceramic, Vol. 12," edited by R. C. Bradt, D. P. H. Hasselman, D. Munz, M. Sakai and V. Ya. Shevchenko (Plenum Publ. Corp., NY, 1996) p. 179.
7. T. OHJI, T. HIRANO, A. NAKAHIRA and K. NIIHARA, *J. Am. Cer. Soc.* **79** (1996) 33–45.
8. T. OHJI and K. NIIHARA, *J. Cer. Soc. Jap.* **104** (1996)581–582.
9. G. PEZZOTTI, V. SERGO, K. OTA, O. SBAIZERO, N. MURAKI, T. NISHIDA and M. SAKAI, *ibid.* **104** (1996) 497–503.
10. M. HOFFMAN and J. RÖDEL, *ibid.* **105** (1997) 1086–1090.
11. S. JIAO, M. L. JENKINS and R. W. DAVIDGE, *Acta Mater.* **45** (1997) 149–156.
12. J. LUO and R. STEVENS, *J. Europ. Cer. Soc.* **17** (1997) 1565–1572.
13. B. R. LAWN, N. P. PADTURE, L. M. BRAUN and S. J. BENNISON, *J. Am. Cer. Soc.* **76** (1993) 2235–2240.
14. M. STERNITZKE, *J. Europ. Cer. Soc.* **17** (1997) 1061–1082.
15. T. MORI and K. TANAKA, *Acta Metall.* **21** (1973) 571–574.
16. R. A. CUTLER and A. V. VIRKAR, *J. Mater. Sci.* **20** (1985) 3557–3573.
17. M. TAYA, S. HAYASHI, A. KOBAYASHI and H. S. YOON, *J. Am. Cer. Soc.* **73** (1990) 1382–1391.
18. C. M. CHIMANI, H. J. BÖHM and F. G. RAMMERSTORFER, *Scripta Mater.* **36** (1997) 943–947.
19. S. SCHMAUDER, in "Fracture Mechanics of Ceramics, Vol. 12," edited by R. C. Bradt, D. P. H. Hasselman, D. Munz, M. Sakai and V. Ya. Shevchenko (Plenum Publ. Corp., NY, 1996) p. 443.
20. J. D. ESHELBY, in "Progress in Solid State Physics, Vol.3," edited by F. Seitz and D. Turnbull (Academic Press, NY, 1956) p. 79.
21. F. F. LANGE, in "Fracture Mechanics of Ceramics, Vol. 2," edited by R. C. Bradt, D. P. H. Hasselman and F. F. Lange (Plenum Publ. Corp., NY, 1974) p. 599.
22. A. G. EVANS, *Acta Metall.* **26** (1978) 1845–1853.
23. D. R. CLARKE, *ibid.* 28 (1980) 913–924.
24. R. W. DAVIDGE, *ibid.* **29** (1981) 1695–1702.
25. Y. M. ITO, M. ROSENBLATT, L. Y. CHANG, F. F. LANGE and A. G. EVANS, *Int. J. Fract.* **17** (1982) 483–491.
26. Y. FU, A. G. EVANS and W. M. KRIVEN, *J. Am. Cer. Soc.* **67** (1984) 626–630.
27. V. TVERGAARD and J. W. HUTCHINSON, *ibid.* **71** (1988) 157–166.
28. Z. LI and R. C. BRADT, *ibid.* **72** (1989) 70–77.
29. N. LAWS and J. C. LEE, *J. Mech. Phys. Solids* **37** (1989) 603–618.
30. S. M. WIEDERHORN, *J. Am. Cer. Soc.* **52** (1969) 485–491.
31. R. M. McMEEKING and A. G. EVANS, *ibid.* **65** (1982) 242–247.
32. D. M. PARKS, *Int. J. Fract* **10** (1974) 487–502.

Received 20 January
and accepted 24 August 1999